Acta Crystallographica Section F
Structural Biology Communications
ISSN 2053-230X

Purification, crystallization and preliminary X-ray diffraction of the N-terminal calmodulin-like domain of the human mitochondrial ATP-Mg/P_i carrier SCaMC1

Qin Yang,* Sven Brüschweiler and James J. Chou*

Biological Chemistry and Molecular Pharmacology, Harvard Medical School, Boston, MA 02115, USA

Correspondence e-mail: yang@crystal.harvard.edu, chou@crystal.harvard.edu

Received 15 October 2013
Accepted 27 November 2013

SCaMC is an ATP-Mg/P_i carrier protein located at the mitochondrial inner membrane. SCaMC has an unusual N-terminal Ca^{2+}-binding domain (NTD) in addition to its characteristic six-helix transmembrane bundle. The NTD of human SCaMC1 (residues 1–193) was expressed and purified in order to study its role in Ca^{2+}-regulated ATP-Mg/P_i transport mediated by its transmembrane domain. While Ca^{2+}-bound NTD could be crystallized, the apo state resisted extensive crystallization trials. Selenomethionine-labeled Ca^{2+}-bound NTD crystals, which belonged to space group $P6_222$ with one molecule per asymmetric unit, diffracted X-rays to 2.9 Å resolution.

1. Introduction

Ca^{2+} is one of the most important secondary signaling messengers and is involved in a wide range of physiological events (Clapham, 2007). These include muscle contraction, permeability of ion channels, induction of mitochondrial permeability transition and apoptosis, RNA processing and many more (Clapham, 2007; Yang & Doublié, 2011). During the study of mitochondrial permeability transition, a related Ca^{2+}-activated ATP-Mg/P_i exchange activity in mitochondria was first described (Nosek *et al.*, 1990), and it was subsequently identified to be mediated by short calcium-binding mitochondrial carriers (SCaMCs; Chen, 2004; del Arco & Satrústegui, 2004; Fiermonte *et al.*, 2004; Mashima *et al.*, 2003).

SCaMCs belong to the mitochondrial carrier family consisting of structurally related transmembrane transporter proteins that shuttle important metabolites, nucleotides and cofactors across the mitochondrial inner membrane (Chen, Li *et al.*, 2012; Klingenberg, 2009; Palmieri, 2008; Walker & Runswick, 1993). SCaMC has an unusual N-terminal domain (NTD) appended to the characteristic six transmembrane helices of mitochondrial carriers (Berardi *et al.*, 2011; Pebay-Peyroula *et al.*, 2003). Primary-sequence analysis revealed that the SCaMC NTD contains four EF-hand Ca^{2+}-binding motifs (Chen, 2004; del Arco & Satrústegui, 2004; Fiermonte *et al.*, 2004; Mashima *et al.*, 2003) and has ∼50% sequence similarity to calmodulin (CaM), a well characterized Ca^{2+}-sensor protein (Chagot & Chazin, 2011; Chou *et al.*, 2001; Hoeflich & Ikura, 2002; Ikura *et al.*, 1992; Kuboniwa *et al.*, 1995). In coherence with the possession of a Ca^{2+}-binding domain, SCaMC-mediated ATP-Mg/P_i exchange is inactive in the resting state (low Ca^{2+} concentration) and is stimulated by increased intracellular Ca^{2+} concentration (Amigo *et al.*, 2013; Cavero *et al.*, 2005; Traba *et al.*, 2012). To better understand the functional role of SCaMC NTD in the Ca^{2+}-mediated carrier activation, we set out to obtain structural information on the NTD in the presence and absence of Ca^{2+}. Several paralogs of SCaMC have been identified in humans, including SCaMC-1/SLC25A24, SCaMC-2/SLC25A25, SCaMC-3/SLC25A23 (Bassi *et al.*, 2005; del Arco & Satrústegui, 2004; Fiermonte *et al.*, 2004; Mashima *et al.*, 2003), SCaMC-1L (Amigo *et al.*, 2012) and SCaMC-3L (Traba *et al.*, 2009). In this report, we describe the preparation, crystallization and X-ray diffraction analysis of human SCaMC1 NTD.

2. Materials and methods

2.1. Cloning, expression and purification of human SCaMC1 NTD

A gene encoding the NTD (residues 1–193) of human SCaMC1 (UniProt ID Q6NUK1) was codon-optimized for expression in *Escherichia coli*, synthesized by GenScript and subsequently cloned into pET-21a expression vector (Novagen) using *Nde*I and *Xho*I restriction-enzyme sites. The NTD was transformed into *E. coli* BL21 (DE3) cells (New England Biolabs) and was expressed using auto-induction at 293 K (Studier, 2005). For purification of the NTD, the cells were lysed and the supernatant was passed through cobalt resin (Clontech; Chen, Gamache *et al.*, 2012) pre-equilibrated with 20 m*M* HEPES–NaOH pH 7.4, 150 m*M* NaCl, 5 m*M* imidazole. The resin was washed in the same buffer with 20 m*M* imidazole. The protein was eluted with 200 m*M* imidazole and was then passed through a HiLoad 16/60 Superdex 75 size-exclusion column (GE Healthcare) in 20 m*M* HEPES–NaOH pH 7.0, 20 m*M* NaCl, 5 m*M* $CaCl_2$. The apo form of NTD was obtained by extensive dialysis against 20 m*M* HEPES–NaOH pH 7.0, 20 m*M* NaCl, 20 m*M* EDTA, 5 m*M* EGTA three times (12 h each) followed by final dialysis against 20 m*M* HEPES pH 7.0, 20 m*M* NaCl, 5 m*M* EDTA. Ca^{2+}-bound and apo NTD were concentrated to 10 mg ml^{-1} using an Amicon YM-10 concentrator (Millipore) and were immediately used for crystallization. A total of 5 mg of purified NTD was obtained from a 1 l culture. Selenomethionine-labeled protein was prepared using a previously published protocol (Doublié, 2007) and was purified as described above.

2.2. Crystallization, data collection and processing

A Mosquito HTS crystallization robot (TTP LabTech) was used to set up 96-well sitting-drop plates (TTP LabTech) by mixing 200 nl NTD solution with 200 nl crystallization solution from the Wizard III and IV crystallization screens (Emerald BioSystems). For Ca^{2+}-bound NTD, crystals were identified in eight of the 96 conditions. Condition No. 56 [100 m*M* Tris pH 8.5, 2 *M* Li_2SO_4, 2%(*w*/*v*) PEG 400], which gave the best initial crystal morphology, was further optimized in a 24-well VDX plate (Hampton Research) by performing several rounds of hanging-drop experiments in which the pH, precipitant concentration and additives were varied. Crystals appeared in 2 d and grew to 0.1 mm in size within one week at 293 K.

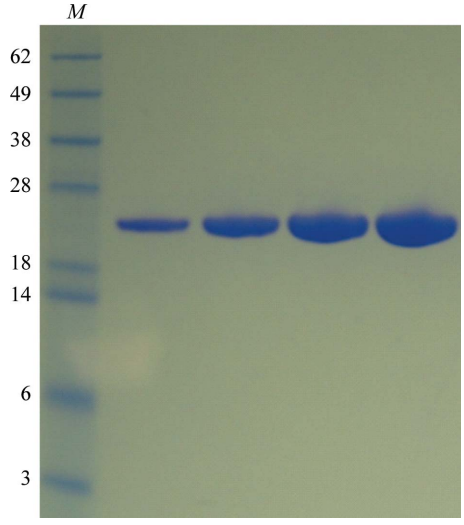

Figure 1
SDS–PAGE of the purified NTD loaded at increased protein concentrations. Lane *M* contains molecular-mass marker (labelled in kDa).

Table 1
X-ray data-collection and processing statistics.

Values in parentheses are for the outermost resolution shell.

	SeMet peak	SeMet inflection	SeMet remote
Data collection			
Wavelength (Å)	0.9794	0.9795	0.9494
Resolution (Å)	40–2.90 (2.98–2.90)	40–2.92 (3.03–2.92)	40–3.00 (3.10–3.00)
Space group	$P6_222$	$P6_222$	$P6_222$
Unit-cell parameters			
$a = b$ (Å)	74.480	74.489	74.503
c (Å)	173.64	173.65	173.71
$\alpha = \beta$ (°)	90	90	90
γ (°)	120	120	120
Total reflections	260454 (20594)	254334 (28333)	235619 (23782)
Unique reflections	11865 (886)	11613 (1220)	10726 (1023)
Multiplicity	21.6 (23.2)	21.9 (23.2)	21.9 (23.2)
$\langle I/\sigma(I)\rangle$	26.89 (5.09)	27.95 (5.74)	27.22 (5.69)
Completeness (%)	99.1 (100)	99.0 (100)	99.2 (100)
R_{merge}† (%)	8.0 (90.8)	7.9 (80.7)	8.1 (86.5)
Phasing			
No. of SeMet sites	4		
Figure of merit (*phenix.autosol*)	0.58		

† $R_{merge} = \sum_{hkl}\sum_i |I_i(hkl) - \langle I(hkl)\rangle| / \sum_{hkl}\sum_i I_i(hkl)$, where $I_i(hkl)$ is the observed intensity and $\langle I(hkl)\rangle$ is the average intensity for multiple measurements.

Crystals were cryoprotected during the course of growth; no further procedure was performed prior to cryocooling in liquid nitrogen (Yang, Gilmartin *et al.*, 2011). For apo-form NTD, several commercial crystallization screen kits, Crystal Screen HT, Index HT, PEG/Ion HT, SaltRx (Hampton Research), Wizard I and II and Wizard III and IV (Emerald BioSystems), were tested. However, no crystals were obtained before the plates completely dried out.

A complete multiple-wavelength anomalous diffraction (MAD) data set was collected on Advanced Photon Source beamline 23-ID-D at Argonne National Laboratory using a MAR 300 CCD detector. Three wavelengths were used for MAD data-set collection: 0.9794 Å (peak), 0.9795 Å (inflection) and 0.9494 Å (remote). The diffraction data were indexed, integrated and scaled using the *HKL*-2000 suite of programs (Otwinowski & Minor, 1997) installed, configured and provided by *SBGrid* (Morin *et al.*, 2013). The NTD structure was solved using *phenix.autosol* (Adams *et al.*, 2010). Crystallographic statistics are shown in Table 1.

3. Results and discussion

3.1. Crystallization of Ca^{2+}-bound SCaMC1 NTD

Full-length human SCaMC1 (also referred to as SLC25A24) consists of 477 residues. A sequence analysis of SCaMC1 using the *MemBrain* transmembrane protein structure prediction server (Shen & Chou, 2008) and sequence alignment with other mitochondrial carrier proteins suggested that the transmembrane domain is composed of residues 194–477. The NTD composed of residues 1–193 and a C-terminal His_6 tag with an expected molecular weight of 22.9 kDa was constructed in order to dissect its functional role in Ca^{2+} sensing. After cobalt resin affinity purification and size-exclusion chromatography, the NTD migrated on SDS–PAGE as a single band with a molecular weight of ∼23 kDa (Fig. 1). For the Ca^{2+}-bound NTD, crystals were obtained in eight of the 96 conditions screened, more specifically Nos. 1, 3, 5, 10, 32, 44, 56 and 60 from the Wizard III and IV screens (Emerald BioSystems). After several rounds of optimization based on condition No. 56, large single crystals (0.1 × 0.03 × 0.01 mm; Fig. 2) were obtained from a hanging drop consisting of 1 µl Ca^{2+}-bound NTD solution (10 mg ml^{-1}) and 1 µl reservoir solution consisting of 50 m*M* Tris pH 7.8, 2 *M* Li_2SO_4, 4%(*w*/*v*) PEG

400 equilibrated against 500 µl reservoir solution at 293 K. Crystals appeared in 2 d and grew to full size in one week. As indicated by the diffraction pattern (Fig. 3), 2 *M* Li_2SO_4 in the reservoir was sufficient to cryoprotect the crystals, similar to previous observations using 2 *M* NaCl as reservoir solution (Yang, Coseno *et al.*, 2011; Yang, Faucher *et al.*, 2011; Yang *et al.*, 2010, 2013). Thus, no additional cryoprotectant solution was needed. Attempts to crystallize NTD in the absence of Ca^{2+} were unsuccessful. In synergy with the success rate of crystallization, the Ca^{2+}-bound NTD is in a compact, more rigid form, whereas the apo NTD is in a flexible, less structured form in solution, as demonstrated by studying the dynamics of NTD using nuclear magnetic resonance (Yang *et al.*, 2014).

3.2. Initial X-ray diffraction analysis

Three complete data sets at different wavelengths were collected using a selenomethionine-labeled crystal that diffracted to 2.9 Å resolution. The data were indexed in space group $P6_222$, with unit-cell parameters $a = b = 74.48$, $c = 173.637$ Å, $\alpha = \beta = 90$, $\gamma = 120^\circ$. The calculated Matthews coefficient (V_M) of 3.20 $Å^3$ Da^{-1}, with a corresponding solvent content of 61%, suggests the presence of one molecule per asymmetric unit (Matthews, 1968). The NTD structure was solved by MAD using *phenix.autosol* (Adams *et al.*, 2010). All four selenomethionine sites were identified. After density modification, 134 of 193 residues were built using *phenix.autobuild* (Adams *et al.*, 2010). Further model building and structural analysis will be reported in a separate paper (Yang *et al.*, 2014).

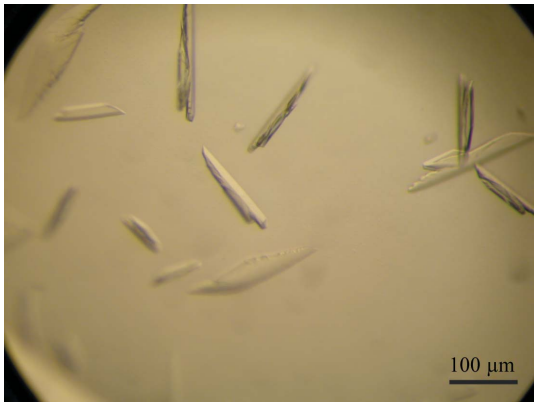

Figure 2
Crystal of Ca^{2+}-bound human SCaMC1 NTD (residues 1–193). The dimensions of the crystals are about 0.1 × 0.03 × 0.01 mm.

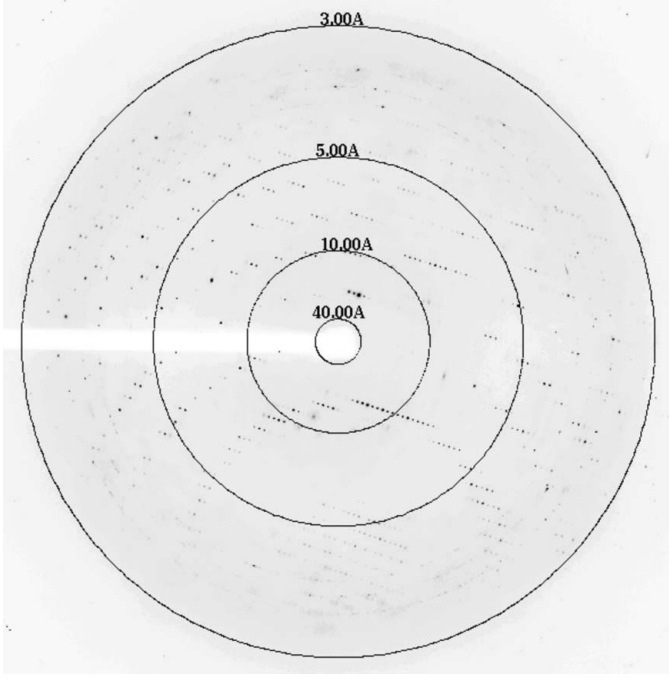

Figure 3
A representative diffraction image of the NTD crystal with a 2.9 Å resolution limit.

We thank members of the Chou laboratory for technical assistance and insightful discussions and Dr Yu Chen (Harvard Medical School) for X-ray data collection. This work is based upon research conducted at the Advanced Photon Source (Northeastern Collaborative Access Team beamlines). SB is the recipient of an Erwin Schrödinger postdoctoral fellowship from the Austrian Science Fund (FWF, J3251). This work was supported by NIH grant No. GM094608 (to JJC).

References

Adams, P. D. *et al.* (2010). *Acta Cryst.* D**66**, 213–221.
Amigo, I., Traba, J., González-Barroso, M. M., Rueda, C. B., Fernández, M., Rial, E., Sánchez, A., Satrústegui, J. & Del Arco, A. (2013). *J. Biol. Chem.* **288**, 7791–7802.
Amigo, I., Traba, J., Satrústegui, J. & del Arco, A. (2012). *PLoS One*, **7**, e40470.
Arco, A. del & Satrústegui, J. (2004). *J. Biol. Chem.* **279**, 24701–24713.
Bassi, M. T., Manzoni, M., Bresciani, R., Pizzo, M. T., Della Monica, A., Barlati, S., Monti, E. & Borsani, G. (2005). *Gene*, **345**, 173–182.
Berardi, M. J., Shih, W. M., Harrison, S. C. & Chou, J. J. (2011). *Nature (London)*, **476**, 109–113.
Cavero, S., Traba, J., Del Arco, A. & Satrústegui, J. (2005). *Biochem. J.* **392**, 537–544.
Chagot, B. & Chazin, W. J. (2011). *J. Mol. Biol.* **406**, 106–119.
Chen, W., Gamache, E., Richardson, D., Du, Z. & Wang, C. (2012). *Protein Expr. Purif.* **81**, 11–17.
Chen, W., Li, L., Du, Z., Liu, J., Reitter, J. N., Mills, K. V., Linhardt, R. J. & Wang, C. (2012). *J. Am. Chem. Soc.* **134**, 2500–2503.
Chen, X. J. (2004). *Genetics*, **167**, 607–617.
Chou, J. J., Li, S., Klee, C. B. & Bax, A. (2001). *Nature Struct. Biol.* **8**, 990–997.
Clapham, D. E. (2007). *Cell*, **131**, 1047–1058.
Doublié, S. (2007). *Methods Mol. Biol.* **363**, 91–108.
Fiermonte, G., De Leonardis, F., Todisco, S., Palmieri, L., Lasorsa, F. M. & Palmieri, F. (2004). *J. Biol. Chem.* **279**, 30722–30730.
Hoeflich, K. P. & Ikura, M. (2002). *Cell*, **108**, 739–742.
Ikura, M., Clore, G. M., Gronenborn, A. M., Zhu, G., Klee, C. B. & Bax, A. (1992). *Science*, **256**, 632–638.
Klingenberg, M. (2009). *Biochim. Biophys. Acta*, **1788**, 2048–2058.
Kuboniwa, H., Tjandra, N., Grzesiek, S., Ren, H., Klee, C. B. & Bax, A. (1995). *Nature Struct. Biol.* **2**, 768–776.
Mashima, H., Ueda, N., Ohno, H., Suzuki, J., Ohnishi, H., Yasuda, H., Tsuchida, T., Kanamaru, C., Makita, N., Iiri, T., Omata, M. & Kojima, I. (2003). *J. Biol. Chem.* **278**, 9520–9527.
Matthews, B. W. (1968). *J. Mol. Biol.* **33**, 491–497.
Morin, A., Eisenbraun, B., Key, J., Sanschagrin, P. C., Timony, M. A., Ottaviano, M. & Sliz, P. (2013). *Elife*, **2**, e01456.
Nosek, M. T., Dransfield, D. T. & Aprille, J. R. (1990). *J. Biol. Chem.* **265**, 8444–8450.
Otwinowski, Z. & Minor, W. (1997). *Methods Enzymol.* **276**, 307–326.
Palmieri, F. (2008). *Biochim. Biophys. Acta*, **1777**, 564–578.
Pebay-Peyroula, E., Dahout-Gonzalez, C., Kahn, R., Trézéguet, V., Lauquin, G. J. & Brandolin, G. (2003). *Nature (London)*, **426**, 39–44.
Shen, H. & Chou, J. J. (2008). *PLoS One*, **3**, e2399.
Studier, F. W. (2005). *Protein Expr. Purif.* **41**, 207–234.
Traba, J., Del Arco, A., Duchen, M. R., Szabadkai, G. & Satrústegui, J. (2012). *Cell Death Differ.* **19**, 650–660.
Traba, J., Satrústegui, J. & del Arco, A. (2009). *Biochem. J.* **418**, 125–133.
Walker, J. E. & Runswick, M. J. (1993). *J. Bioenerg. Biomembr.* **25**, 435–446.
Yang, Q., Brüschweiler, S. & Chou, J. J. (2014). *Structure*, doi:10.1016/j.str.2013.10.018.

Yang, Q., Coseno, M., Gilmartin, G. M. & Doublié, S. (2011). *Structure*, **19**, 368–377.
Yang, Q. & Doublié, S. (2011). *Wiley Interdiscip. Rev. RNA*, **2**, 732–747.
Yang, Q., Faucher, F., Coseno, M., Heckman, J. & Doublié, S. (2011). *Acta Cryst.* F**67**, 241–244.
Yang, Q., Gilmartin, G. M. & Doublié, S. (2010). *Proc. Natl Acad. Sci. USA*, **107**, 10062–10067.
Yang, Q., Gilmartin, G. M. & Doublié, S. (2011). *RNA Biol.* **8**, 748–753.
Yang, Q., Nausch, L. W. M., Martin, G., Keller, W. & Doublié, S. (2013). *J. Mol. Biol.*, doi:10.1016/j.jmb.2013.09.025.